Volume 1 | Number 1 | Jan 2013 | Pages 1–100

Nanoscale

www.rsc.org/nanoscale

ROYAL SOCIETY OF CHEMISTRY

www.rsc.org/nanoscale

Nanoscale

Dynamic Article Links ▶

PAPER

Efficiency enhancement in Cu_2ZnSnS_4 solar cells with subwavelength grating nanostructures

Shou-Yi Kuo[a,b] and Ming-Yang Hsieh[a]

In the article, a study is presented of sub-wavelength grating (SWG) nanostructures for broadband and omni-directional anti-reflection coatings (ARCs) on Cu_2ZnSnS_4 (CZTS) solar cells using the rigorous coupled-wave analysis (RCWA) method. Various SWG nanostructures of different shapes and periodic on CZTS solar cells are discussed in detail. The optimized reflectance decreased to 1.67%, and efficiency
10 increased to 13.74%, accordingly. The omni-directional and broadband antireflections of the SWG nanostructures are also investigated. Under a simulated 1-sun condition and light incident angle increased to 80°, cells with SWG nanostructures enhanced the short-circuit current density by 16.5%. This considerable enhancement in light harvesting is attributed to the linearly graded effective refractive index profile from the air to the device surface.

Introduction

15   Anti-reflection coatings (ARCs) play an important role in the performance of optoelectronic devices because of their ability to minimize Fresnel reflection loss at the interface between air and semiconductor materials, such as optical components,
20 photovoltaic systems, and light-emitting diodes (LEDs) [1-6]. Single-layer or multilayer stacks of film were traditionally used for ARCs in the narrow ranges of incident wavelengths and angles, such as silicon nitride or silicon dioxide [7-8]. However, they continue to have certain disadvantages, such as material
25 selection, thermal mismatch-induced lamination, and accurate thickness control [9]. Since sub-wavelength grating (SWG) structures of moth-eye pillars were discovered by Bernhard in 1967, the function of these nipple-array structures has been suggested as the ultimate solution to suppress light reflection in
30 the entire solar radiation spectrum. The origin of these antireflective properties emerged from a continuous gradient of the refraction index between air and the corneal surface. In the past few years, for optimizing the efficiency of optical devices, the behavior of light trapping in nanostructures has been
35 investigated intensively. For example, surface profile, diameter, and length-dependent, light trapping properties of nanorod arrays have been investigated thoroughly for the design and optimization of the light trapping scheme. The alignment variation of nanowires and interfaces (between air/NWA layers
40 and NWA layers/substrates) plays an important role in surface reflection and light scattering [10-11].Therefore, antireflective SWG structures have attracted interest in their employment in optoelectronic devices as an alternative to multilayer ARCs [12-18].
45   Solar cells can be categorized as bulk or thin-film solar cells by their structures. In thin-film solar cells, chalcogenide-based

materials, such as $CuInSe_2$ (CIS), $Cu(In,Ga)Se_2$ (CIGS), and CdTe, have attracted considerable interest because of their high absorption coefficient and high-power conversion efficiency [19,
50 20]. However, these materials have certain limitations, such as the scarcity of indium and gallium, and the environmental issues associated with Se. Therefore, Cu_2ZnSnS_4 (CZTS) is considered the most promising alternative compound for the following reasons. The expensive indium was replaced by economical zinc,
55 and gallium was replaced by tin. In addition, the p-type CZTS has a direct optical tunable band-gap in the range of 1.4 - 1.56 eV, and a large absorption coefficient over 10^4 cm^{-1}. The power conversion efficiencies of the CZTS solar cells have exceeded 11%, which is a record efficiency for electrodeposited CZTS
60 solar devices [21]. Therefore, CZTS has the greatest potential as the next generation of photovoltaic devices.
    Using the transparent conductive oxide (TCO) layer as a window layer is important, and is widely used in optoelectronic devices. The CZTS solar cell is structurally similar to CIGS solar
65 cell. The material of transparent conducting oxide (TCO) layer in CIGS solar cell is aluminum-doped zinc oxide (AZO) or indium tin oxide (ITO) [22,23]. However, AZO is a wide direct band-gap (3.3 eV) semiconductor, and is a promising alternative to ITO as a TCO for optoelectronic devices because of its advantages,
70 including low cost, non-toxicity, and excellent chemical and thermal stability [24-28]. Therefore, the industrial processes of mature CIGS-based cells are expected to be applied on CZTS-based cells, including aluminum-doped zinc oxide (AZO). At this stage, we have concentrated on the simulation of AZO layer with
75 practicable subwavelength structures.
    In previous works, the synthesis of CZTS thin films using various vacuum and non-vacuum techniques have been reported [29-31]. Recently, Winkler et al. reported the design approach combines optical modeling of idealized planar devices with a

semi-empirical approach for treating the impact of surface roughness [32]. Malekmohammad et al. reported that broadband antireflection layers have been fabricated by two dimensional (2D) photonic crystals (PCs) with tapered pillars on the Si substrate,
5 and that produced by interference lithography and reactive ion etching (RIE) techniques [33]. However, no detailed investigations have been conducted on CZTS solar cells with AZO SWG nanostructures, and there are few literatures systematically discussing the SWG nanostructures and electrical
10 properties on other photovoltaic devices. In this study, we have made a detailed and systematic study of CZTS solar cells with SWG nanostructures. The electrical and optical properties of SWG nanostructures with various shapes, thicknesses, and sizes have been investigated. The rigorous coupled-wave analysis
15 (RCWA) method was used to simulate the optical antireflection characteristics of the AZO SWG nanostructures on CZTS solar cell. The CZTS solar cells normally consist of a CdS buffer layer deposited onto a CZTS absorber layer, and a highly resistive ZnO layer was introduced between the CdS and AZO to prevent
20 leakage current. The molybdenum (Mo) is normally used as back contact for CZTS solar cells due to it has low resistivity, high melting point, excellent chemical stability and good adhesion between absorption layer and soda-lime glass. Therefore, the multi-layered structure of CZTS solar consisted of
25 AZO/ZnO/CdS/CZTS/Mo on a soda-lime glass substrate. The omnidirectional and broadband antireflections of the AZO SWG nanostructures are also investigated. The optimization of the SWG nanostructures promises a superior photocurrent generation over an entire day and replaces the sunlight tracking system.

30 ## Simulation

The theoretical analysis of the optical characteristics in the CZTS solar cells with AZO SWG nanostructures was performed by the RCWA method, which simulation program was developed by RSoft Design Group, Inc. The device characteristics of the
35 CZTS solar cells are studied numerically using the APSYS simulation program, which was developed by Crosslight Software Inc[34]. The APSYS simulation program can deal with electrical properties by solving several interwoven equations including the basic Poisson's equation, drift-diffusion equations, photon rate
40 equation, and scalar wave equation. In the simulations, the CZTS solar cell structure contains several layers, including a 300-nm-thick AZO TCO layer (electron concentration:$3*10^{20}$ cm^{-3}), a 50-nm-thick intrinsic ZnO layer (electron concentration:$5*10^{17}$ cm^{-3}), a 50-nm-thick CdS buffer layer (electron concentration:$1*10^{17}$
45 cm^{-3}), a 2000-nm-thick CZTS absorber layer(hole concentration:$1*10^{16}$ cm^{-3}), a 500-nm-thick Mo bottom contact, and a glass substrate that comprises the CIGS solar cell structure. The device geometry is a square shape of 100 μm×100 μm with electrode coverage of 10%, and we assume the contacts are ideal
50 ohmic. It was assumed that the interfaces in the CZTS solar cell are specular, and that the unpolarised incident light entered from the air into the solar cell. For the constituent materials used in the numerical modeling of a CZTS solar cell, the physical information was employed according to literature that included
55 their refractive indices and extinction coefficients [35,36]. Table I shows the basic parameters of the AZO, i-ZnO, CdS, and CZTS layers for the simulations. In addition, all simulations were performed under one sun standard air mass 1.5 global (AM1.5g,

100mW/cm^2) light spectrum and room temperature. For the AZO
60 nanostructures on the CZTS solar cell, the optimization was progressed by a sequential design. In this simulation, first, the order of taper (O$_T$) of the AZO SWGs was designed. The geometry was then designed of the AZO SWGs. Furthermore, omni-directional antireflection characteristics were also
65 investigated with the incident angle varied from 0° to 80°.

Results and discussion

For the 3D numerical modeling of the AZO SWG nanostructures on the CZTS solar cell, the periodic geometry was represented in the Cartesian coordinate system by a scalar-valued
70 function of three variables f(x, y, z). The various-shaped nanostructures are defined by O$_T$ in the equations as follows:

$$r = (H-z)^{\frac{1}{O_T}} + R \ and \ x^2 + y^2 = r^2 \ (0 \le z \le H) \ (1)$$

where r is the radius of circle in XY-plane, and H and R are the
75 height and the bottom radius of the AZO SWGs, respectively. The usual geometry of AZO SWG is expressed by the equation shown in Fig. 1(a). By determining r by varying the z value from 0 to H, the 3D geometry of SWG was established. Fig. 1(b), shows the geometries of AZO SWGs in hexagonally close-
80 packed arrays at O$_T$ = 0.5, 1, 1.6, 2, and 3. For O$_T$ ≥ 2, the equation provides parabolic-shaped geometries, and it changes to a conical shape at O$_T$ = 1. For O$_T$ < 1, the geometry of the conical shape becomes needle-shaped. In addition, the effective refractive index (n$_{eff}$) of the AZO SWG structures can be calculated from
85 the volume fraction of the AZO SWG structures using effective-medium theory [37]:

$$n_{eff} = \left[n_{AZO}^2 \times f + n_{air}^2 (1-f) \right]^{\frac{1}{2}} \ (2)$$

where f is the filling factor of the AZO SWGs, and n$_{AZO}$ and nair
90 are refractive indexes of AZO and air, respectively. In the calculations, the refractive index of AZO is 2.1 and the AZO SWGs with R = 150 and H = 300 nm at O$_T$ = 0.5, 1, 1.6, 2, and 3 are shown in Fig. 1(c). In previous theoretical papers, the refractive index increased gradually from the air to the device
95 surface, which could efficiently suppress the Fresnel reflection [38, 39]. For O$_T$ = 1, 1.6, and 2, the refractive index increased in a nearly linear gradient from the air to the device surface, and for O$_T$ = 0.5 and 3, the refractive index of AZO SWGs exhibited a nearly exponentially or logarithmically increase from the device
100 surface to the air.

Table I Base parameters for CZTS solar cell

	AZO	i-ZnO	CdS	CZTS
thickness(nm)	300	50	50	2000
ε	9	9	10	10
μ$_n$ (cm^2/V s)	50	50	10	100
μ$_p$ (cm^2/V s)	5	5	1	25
N$_A$ (1/cm^3)	0	0	0	1×10^{16}
N$_D$ (1/cm^3)	3×10^{20}	5×10^{17}	1×10^{17}	0
E$_g$ (eV)	3.3	3.3	2.4	1.44
χ (eV)	4	4	3.75	4.1

ε, dielectric constant; *μ$_n$*, electron mobility;*μ$_p$*, hole mobility; *N$_A$* , effective density of states in conduction band; *N$_D$*, effective density of
105 states in valence band; *E$_g$*, band gap energy and *χ*, electron affinity.
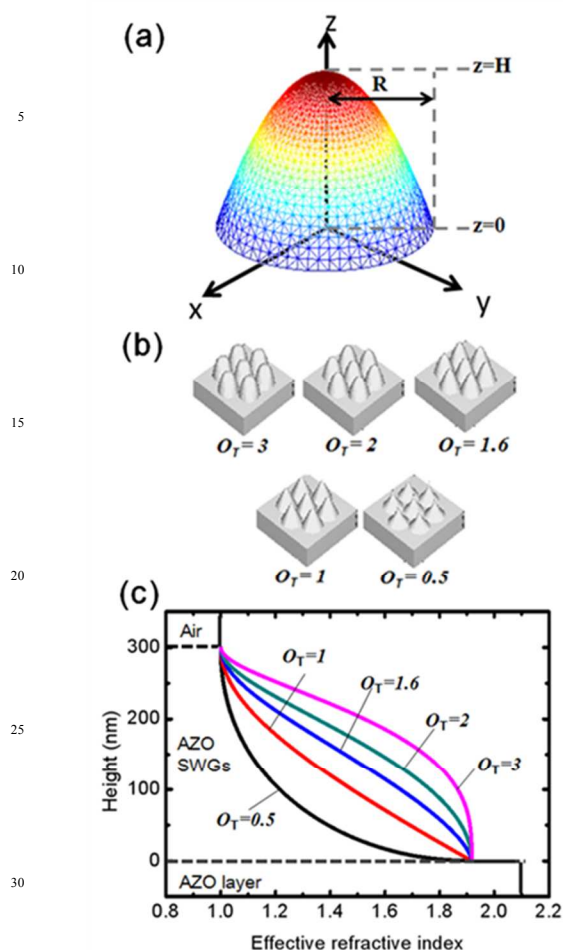
Fig. 1. (a) The geometry of AZO SWGs expressed by the equation of the parabola-shaped, (b) the geometries of AZO SWGs at O_T = 3, 2, 1.6, 1 and 0.5, (c) calculated effective refractive index profiles of the AZO SWGs with R=150 nm and H=300 nm at O_T = 3, 1.6, 2, 1 and 0.5.
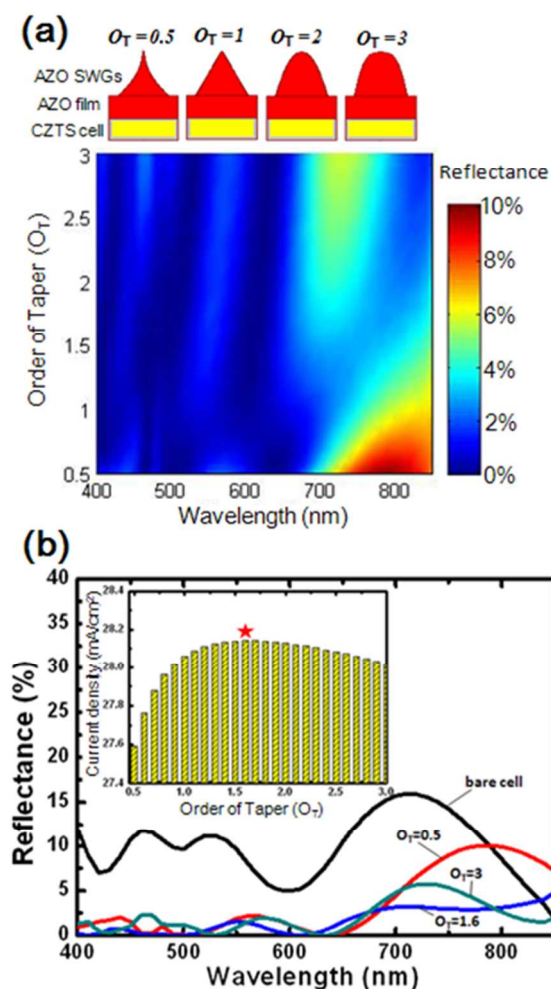
Fig. 2(a) shows the simulated reflectance variation as a function of wavelength at different O_T for the AZO SWG nanostructures, and the simulation models used in the theoretical calculations are also shown. In the simulations, the reflection property was investigated using the RCWA method at wavelengths of 400-850 nm, and the height, period, and the bottom radius of the AZO SWGs were set to 300, 300, and 150 nm, respectively. When the O_T increased from 0.5 to 1.6, the reflectance generally reduced in the wavelength range of 680-800 nm. This is because the parabolic-shaped structures provide a linearly graded effective refractive index profile from the air to the device surface. Additionally, the reflectance of the bare CZTS solar cell is very low (less than 2%) in the wavelength range of 400-680 nm. Therefore, the reflectance generally reduced only in the wavelength range of 680-800 nm. When the O_T increased from 1.6 to 3, the reflectance was increased in wavelength regions of 650-800 nm. This is because the highly tapered needle-shaped structure and strongly parabolic-shaped structure cannot provide a more linearly graded effective refractive index profile from the air to the device surface.

Fig. 2(b) shows the calculated reflectance spectra of the AZO SWGs at O_T = 0.5, 1.6, and 3. When the O_T = 1.6, the average reflectance value is 1.67% in the wavelength range of 400 - 850 nm. The value (O_T = 1.6) is lower than the O_T = 0.5, and 3, and the average reflectance was 3.63% and 2.1%, respectively.

To investigate the optimization of O_T, the current density is calculated as a function of O_T varying between 0.5 and 3, as shown in the inset of Fig. 2(b). Assuming the absorption of photons can be transferred to be electrons completely, the resulting of current density is calculated as follows:

$$J_{sc} = \frac{e}{hc} \int_{400nm}^{850nm} \lambda [1 - R(\lambda)]\, I_{AM1.5G}\, d\lambda \qquad (3)$$

where e is the electron charge, h is the Planck constant of the speed of light, λ is the wavelength, $R(\lambda)$ is the calculated reflectivity for wavelengths between 400 - 850 nm, and $I_{AM1.5G}$ is the intensity of the AM 1.5G solar spectrum. In addition, the multiple reflections and interference have also been considered.

Fig. 2. (a) Contour plots of the calculated reflectance variation as a function of wavelength at different O_T for AZO SWG nanostructures on CZTS solar cell. The simulation models used in these calculations are also shown. (b) Calculated reflectance spectra of bare cell and the AZO SWGs at O_T = 3, 1.6 and 0.5. The inset of (b) reveals the calculated short-circuit current density for different O_T of AZO SWGs on CZTS solar cell.
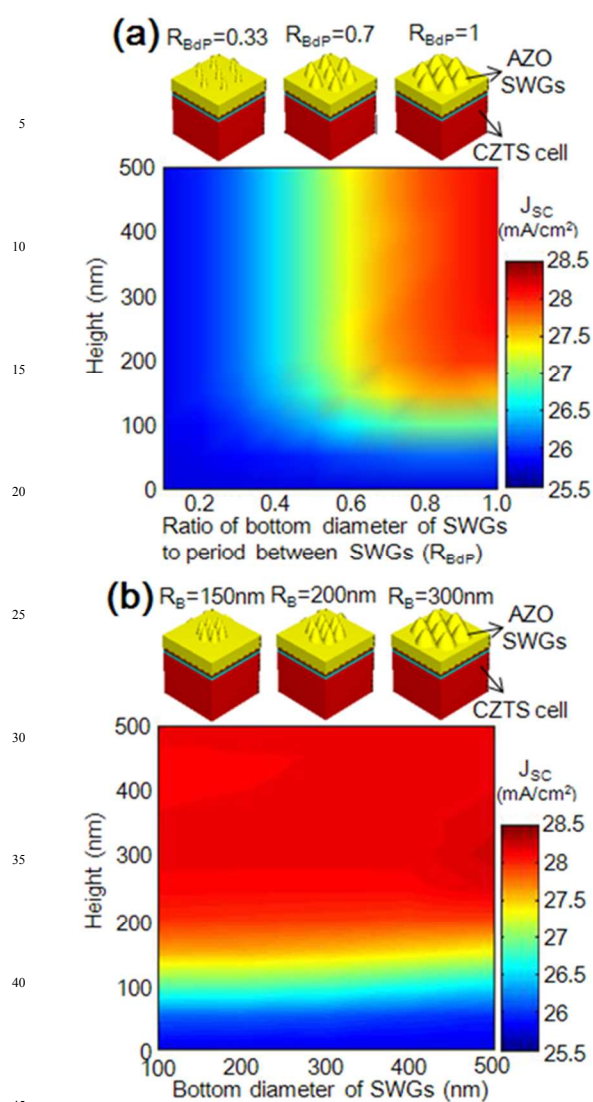
Fig. 3. Contour plots for the calculated short-circuit current density as a function of (a) the R_{BdP} and heights (b) R_B and heights of AZO SWG nanostructures on CZTS solar cell.

According to the simulation, an O_T value of 1.6 was chosen to achieve a relatively high current density for the AZO SWG. After determining the optimal SWG shape, the function of the height of AZO SWG structure, the ratio of the bottom diameter of the SWGs to the period between SWGs (R_{BdP}), and various sizes of AZO SWGs were also explored.

Fig. 3(a) shows that the current density is also strongly affected by R_{BdP} and the height of the AZO SWG structure; the simulation models used in the theoretical calculations are also shown. In the simulation, the O_T value of the AZO SWGs was set to 1.6. The current density was increased when increasing R_{BdP} from 0.1 to 1, which was caused by the increase in the density of SWGs [40]. For R_{BdP} values less than 0.4, the current densities were less than 26.8 mA/cm^2. This is because of the destructive interference caused by multiple reflections of the light at the interfaces of the air/AZO SWG and several layers in the CZTS solar cell structure, where the phases of the waves canceled one another partially or wholly. As the height was increased, the current density was also increased. For heights above 200 nm, current density values of >

27 mA/cm^2 were obtained. Obviously, the higher height can improve the effective refractive index gradient suppressing the surface reflection, and increase the current density because of the smoother grading in effective refractive index profile between the AZO SWG structure and the air. Therefore, the parabolic-shaped AZO SWG nanostructures with a high density and heights above 200 nm can efficiently suppress optical loss. Fig. 3(b) shows the simulated current density variation as a function of the bottom of diameter (R_B) varying between 100 - 500 nm, and the height varying between 0 - 500 nm for AZO SWG nanostructures; the simulation models used in the theoretical calculations are also shown. In the simulations, the R_{BdP} and O_T of the AZO SWGs were set to 1 and 1.6, respectively. Little effect was observed on the current density when the R_B of the parabolic-shaped AZO SWG nanostructures varied between 100 - 500 nm. This is because the similar refractive index grading from the air to the device of the different R_B of the parabolic-shaped AZO SWG. Thus, the optimal AZO SWG structure was determined at $O_T =$ 1.6, R = 150 nm, H = 300 nm, and $R_{BdP} = 1$.

Taking the sun's movement into consideration, it is important that the desired ARCs increase transmission into the absorption layer and minimize the Fresnel reflection omnidirectionally. However, to further understand the omnidirectional AR characteristics, the angle-dependent reflection on the CZTS solar cells was simulated. Fig. 4(a) shows the simulated angle-dependent reflectance of CZTS solar cells with flat (bare cells) and optimal AZO SWG structures, respectively. The angle-dependent mappings are simulated at incident angles between 0° and 80°, and the reflectance spectra are conducted at wavelengths from 400 to 850 nm. Red and blue in the color bar represent the values of reflectance from high to low. Fig 4(a) shows that the reflection of bare cells in the visible range has amplitude in the interference fringe and a higher reflection at 60° - 80°. Afterward, as the optimal AZO SWG structure pattern on the CZTS solar cell surface, the reflection decreased omnidirectionally. These different reflectance behaviors in the angle-dependent mappings are because of the gradual refractive index from the air to the cell surface. Consequently, in the angle-dependent mappings, the CZTS solar cell with the AZO SWG stuctures not only successfully reduces broadband reflectivity but also reduces reflectance for incident angles from 0° to approximately 80°.

To compare the angle-dependence of solar power harvesting and investigate the effect of solar power harvest for an entire day, the solar-spectrum weighted reflectance (SWR) can be calculated by the solar spectral photon flux and the reflectance spectra integrated over a wavelength range of 400 - 850 nm. In the simulation, the following equation was used to express the antireflctive power:

$$SWR = \frac{\int_{400nm}^{850nm} R(\lambda) I_{AM1.5G}(\lambda) d\lambda}{\int_{400nm}^{850nm} I_{AM1.5G}(\lambda) d\lambda} \quad (4)$$

where $I_{AM1.5G}$ is the photon flux density of the AM1.5G solar spectrum, and $R(\lambda)$ is the simulated reflctivity, as shown in Fig 4(a). Fig. 4(b) shows that at normal incidence, the weight reflectance of the bare CZTS cell is approximately 9.92%, whereas the weight reflectance of the cell with the optimal AZO SWG structure on the surface decreases to approximately 1.5%.

In addition, at an incident angle of 70°, the weighted reflectance of the cell with the AZO SWG structure is still less than 12%. This shows that the AZO SWG structure is a suitable alternative to omnidirectional AR coating for CZTS solar cells.
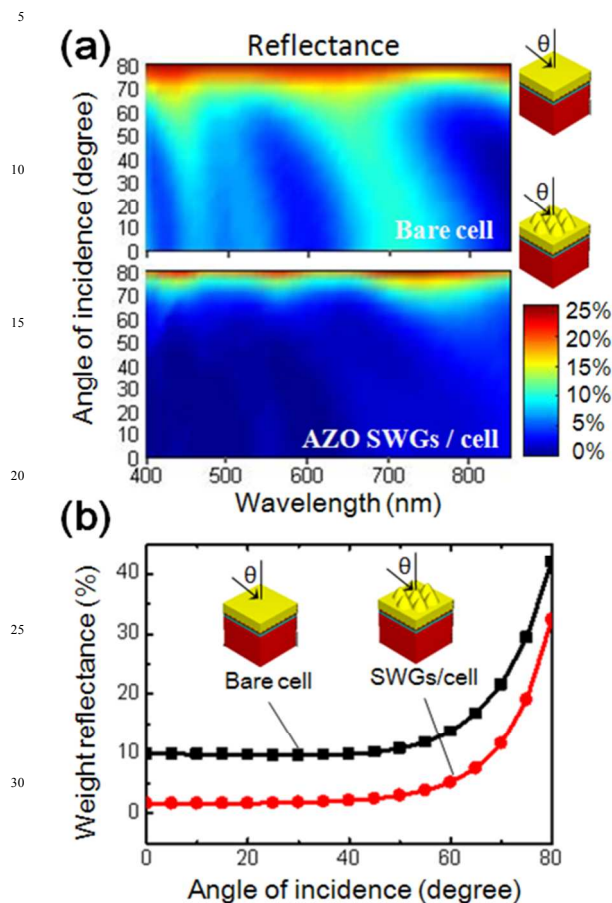
Fig. 4. (a) The simulation angular reflectance spectra for solar cell with (top) bare and (bottom) with AZO SWGs solar cells. (b) The weighted reflectance of the cells.

Fig. 5 shows the influence of the AZO SWGs as an antireflective layer on CZTS solar cell performance. Fig. 5(b) shows the current-voltage (J-V) curves of the solar cells with and without AZO SWGs at a normal incident angle. In the simulation, the optimal AZO SWG structure was applied on the top of the CZTS solar cells for better antireflection; theoretical modeling and simulations of the CZTS solar cell structure were then performed using the APSYS simulation program in the wavelength region of 400 - 850 nm under a standard test condition with simulated air mass of 1.5 global illumination. The device characteristics are shown in the inset of Fig. 5(b). The short-circuit current density increased from 25.7 to 28.1 mA/cm^2 when the CZTS solar cell with the optimal AZO SWG structure, and the open voltages (V$_{OC}$) and fill factors (F.F.) were kept at same values. Our previous study has shown that the shunt resistances and series resistances in CIGS solar cells (bare cell and cell with SWGs) were approximately kept at similar values [17]. As shown in Fig. 5(a), AZO nanostructures were patterned on the surface of cells except the top electrode. Accordingly, it is reasonable that Voc and F.F. values are unaffected by SWGs

process. Moreover, because of the increase in the short-circuit current; the CZTS solar cell with the AZO SWG structure enhanced the power conversion efficiency from 12.56% to 13.74%. Fig. 5(c) shows the short-circuit current density and corresponding enhancement factor (EF$_{jsc}$) of the CZTS solar cells as a function of the incident angle. Because of the increased reflection loss when the incident angle increases, the current density of the solar cells with flat surfaces drops rapidly.

However, in the AZO SWG-integrated solar cell, the current density drops slowly. The EF$_{jsc}$ was defined to express the enhancement of the short-circuit current density of the ARC as follows:

$$EF_{jsc} = \frac{\Delta J_{sc}}{J_{sc}} = \frac{J_{sc}(\text{with SWG}) - J_{sc}(\text{without SWG})}{J_{sc}(\text{without SWG})} \quad (5)$$
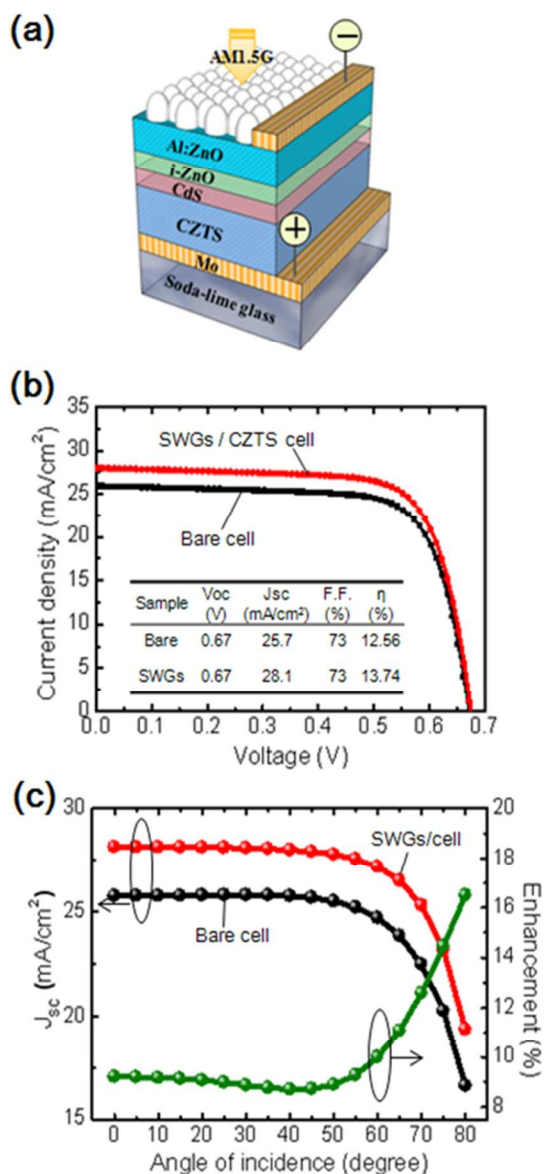
Fig. 5(c) shows the incident angles simulated from 0° to 80°. For the cells simulated at the normal incident angle, the EF$_{jsc}$ is 9.33%. However, when the light incident angle was increased to 80°, the EF$_{jsc}$ increased to 16.5%. Therefore, the AZO SWG structure for antireflection has the most potential to provide enhanced broadband and omni-directional antireflective properties, and that could further improve conversion efficiency over the entire day. Enhanced photovoltaic performance of CZTS solar cell with AZO SWGs has been demonstrated by simulation, and SWGs can be in mass production by holographic lithography or dry etching. Thus it is practical to apply AZO SWGs on CZTS devices.

Conclusions

The SWG nanostructures on the CZTS solar cells were designed and optimized for broadband and omni-directional antireflection. The SWG nanostructure was optimized by varying its shape and geometry using the RCWA method. The results show that optical reflectance can be decreased and the short-circuit current density increased accordingly, by using close-packed patterns. Under optimum conditions, the weight reflectance of the CZTS solar cell with a nipple-shaped SWG nanostructure was significantly reduced from 9.92% to 1.5%, which was calculated over a wavelength range of 400 - 850 nm. Therefore, the photocurrent density increased from 25.7 to 28.1 mA/cm^2, and differed by an additional 2.56 mA/cm^2. For the omnidirectional AR characteristics, the weight reflectance of the cell with the optimal SWG structure at an incident angle of 70° was still less than 12%, and that of the flat cell was 21.6%. In addition, as the light incident angle increased to 80°, the EF$_{jsc}$ was increased to 16.5%. According to these results, the fabrication of SWG nanostructures is an effective approach to improve the conversion efficiency of CZTS solar cells.

Fig. 5. (a) Schematic of CZTS solar cell with AZO nanostructures. (b)The current density-voltage curves of the solar cell with AZO SWGs and the bare cell. (c) The angular photocurrent characterization of the solar cell with AZO SWGs and the bare cell. The green curve shows the corresponding enhancement factor at different incident angles.

Notes and references

ᵃ Department of Electronic Engineering, Chang Gung University, 259 Wen-Hwa 1st Road, Kwei-Shan, Taoyuan 333, Taiwan . Fax: +886-3-2118507; Tel: +886-3-2118800#3351;E-mail: sykuo@mail.cgu.edu.tw.
ᵇ Green Technology Research Center, Chang Gung University, 259 Wen-Hwa 1st Road, Kwei-Shan, Taoyuan 333, Taiwan

1 T. Lohmuller, M. Helgert, M. Sundermann, R. Brunner and J. P. Spatz, Nano Lett., 2008, **8**, 1429.
2 S. Chhajed, M. F. Schubert, J. K. Kim and E. F. Schubert, Appl. Phys. Lett., 2008, **93**, 251108.
3 F.-I. Lai, W.-Y. Chen, C.-C. Kao, H.-C. Kuo and S.-C. Wang, Jpn. J. Appl. Phys., 2006, **45**, 6927
4 Y. M. Song, S. J. Jang, J. S. Yu, and Y. T. Lee, Small, 2010, **6**, 984–987
5 S. Walheim, E. Schaffer, J. Mlynek, and U. Steiner, Science, 1999, **283**, 520–522.
6 Y.-F. Huang, S. Chattopadhyay, Y.-J. Jen, C.-Y. Peng, T.-A. Liu, Y.-K. Hsu, C.-L. Pan, H.-C. Lo, C. H. Hsu, Y. H. Chang, C.-S. Lee, K.-H. Chen, and L.-C. Chen, Nat. Nanotechnol. 2007, **2**, 770–774.
7 M.-A. Tsai, P.-C. Tseng, H.-C. Chen, H.-C. Kuo, and P. Yu, 2011, Opt. Express, **19**, A28–A34.
8 D. Poitras and J. A. Dobrowolski, Appl. Opt. 2004, **43**, 1286–1295.
9 E. Oliva, F. Dimroth, and A. W. Bett, Prog. Photovol. 2008, vol. 16, **4**, 289–295.
10 Y.R. Lin, K. Y. Lai, H. P. Wang, J. H. He, Nanoscale, 2010, 2, 2765-2768.
11 L. Hu and G. Chen, Nano Lett., 2007, 7, 3249
12 J. Zhu, Z. F. Yu, G. F. Burkhard, C. M. Hsu, S. T. Connor, Y. Q. Xu, Q. Wang, M. McGehee, S. H. Fan, and Y. Cui, Nano Lett. 2009, **9**,.279–282.
13 C. J. Ting, M. C. Huang, H. Y. Tsai, C. P. Chou, and C. C. Fu, Nanotechnology 2008, **19**, 205301.
14 B. Paivanranta, T. Saastamoinen, and M. Kuittinen, Nanotechnology 2009, **20**, 375301.
15 Q. Chen, G. Hubbard, P. A. Shields, C. Liu, D. W. E. Allsopp, W. N. Wang, and S. Abbott, Appl. Phys. Lett. 2009, **94**, 263118.
16 J. Y. Chen, W. L. Chang, C. K. Huang, and K. W. Sun, Opt. Express 2011, **19**, 14411–14419.
17 M.Y. Hsieh , S.Y. Kuo , H.V. Han , J. F. Yang , Y. K. Liao , F.I Lai and H. C. Kuo, Nanoscale, 2013, **5** , 3841.
18 S.Y. Kuo , M.Y. Hsieh ,H.V. Han , F.I Lai , Y.L.Tsai, J. F. Yang , T.Y. Chuang and H. C. Kuo, Nanoscale,2013, **5**, 4270.
19 K. Jimbo, R. Kimura, T. Kamimura, S. Yamada, W. S. Maw, H. Araki, K. Oishi, and H. Katagiri, Thin Solid Films, 2007, 5997–5999.
20 D. B. Mitzi n, O. Gunawan, T. K. Todorov, K. Wang, S. Guha, Sol. Energy Mater. Sol. Cells, 2011, **95**, 1421 (2011).
21 T. K. Todorov, J. Tang, S. Bag, O. Gunawan, T. Gokmen, Y. Zhu, D. B. Mitzi, Adv. Energy Mater. 2013, **3**, 34.
22 H. Katagiri, K. Jimbo, S. Yamada, T. Kamimura, W. S. Maw, T. Fukano, T. Ito, and T. Motohiro, Applied Physics Express, 2008, 1 , 041201
23 F. Biccari, R. Chierchia, M. Valentini, P.Mangiapane, E. Salza, C. Malerba, C. Leonor, A. Ricardo, L. Mannarino, P. Scardi, A. Mittiga, Energy Procedia, 2011,10,187-191
24 J.W. Leem ,D.H. Joo ,J.S. Yu, Sol. Energy Mater. Sol. Cells,,2011,95, 2221-2227
25 J. W. Leem, Y. M. Song, Y. T. Lee, J. S. Yu, Applied Physics B, 2010, 99,695-700
26 Z. B. Ayadi, L. E. Mir, K. Djessas, S. Alaya, Nanotechnology 2007, **18**, 445702.
27 M. M. Islama, S. Ishizuka, A. Yamada, K. Matsubara, S. Niki, T. Sakurai, K. Akimoto, Appl. Surf. Sci. 2011, **257**, 4026–4030.
28 S. Y. Kuo, K. C. Liu, F.-I Lai, J. F. Yang, W. C. Chen, M. Y. Hsieh, H.-I Lin and W. T. Lin, Microelectron. Reliab. 2010, **50**, 730.
29 T. Kobayashi, K. Jimbo, K. Tsuchida, S. Shiboda, T. Oyanagi, H. Katagiri, Jpn. J. Appl. Phys.,2005, **44**, 783–787.
30 H. Katagiri, K. Jimbo, S. Yamada, T. Kamimura, W.S. Maw, T. Fukano, T. Ito, T. Motohiro, Appl. Phys. Exp., 2008, **1,** 041201–041202
31 B.H. Shin, O. Gunawan, Y. Zhu, N.A. Bojarczuk, S.J. Chey, S. Guha, Prog. Photovoltaics Res. Appl.,2011, **2** ,1174–1180.
32 M. T. Winkler, W. Wang, O. Gunawan, H. J. Hovel, T. K. Todorov, D. B. Mitzi, Energy Environ. Sci., 2014, **7**, 1029.
33 M. Malekmohammad, M. Soltanolkotabi, A. Erfanian, R. Asadi, S. Bagheri, M. Zahedinejad, M. Khaje, M. H. Naderi, J. Europ. Opt. Soc. Rap. Public. 2012, **7**, 12008.
34 APSYS by Crosslight Software Inc., Burnaby, Canada [Online]. Available: http://www.crosslight.com
35 S. Levcenko, G. Gurieva, M. Guc, and A. Nateprov, Moldavian Journal of the Physical Sciences, 2009, **8**, N2.
36 C.H. Huang, Journal of Physics and Chemistry of Solids, 2008, **69**, 779.
37 J. Zhong, H. Chen, G. Saraf, Y. Lu, C. K. Choi, J. J. Song, D. M. Mackie, and H. Shen, Appl. Phys. Lett., 2007, **90**, 203515.
38 N. D. Arora, J. R. Hauser, J. Appl. Phys. 1982, **53**, 8839–8846.

39 B. K. Shin, T. I. Lee, J. Xiong, C. Hwang, G. Noh, J. H. Cho, J. M. Myoung, Sol. Energy Mater. Sol. Cells, 2011, **95**, 2650–2654.
40 J. W. Leem, Y. P. Kim, and J. S. Yu, J. Opt. Soc. Am. B. 2012, **29**,.357–362.

5

Nanoscale Accepted Manuscript